

Population Branching in the Conical Intersection of the Retinal Chromophore Revealed by Multipulse Ultrafast Optical Spectroscopy

Goran Zgrablić,^{*,†} Anna Maria Novello,^{†,§} and Fulvio Parmigiani^{†,‡}

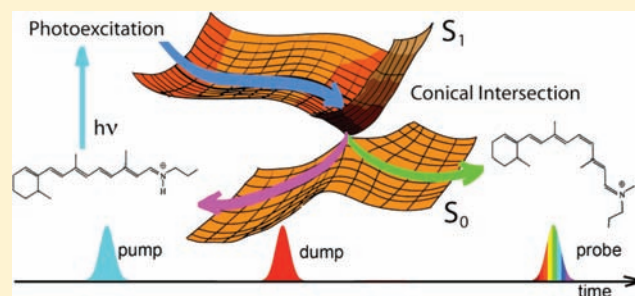
[†]T-ReX Laboratory, Sincrotrone Trieste, S.S. 14 km 163.5 in Area Science Park, I-34012 Basovizza Trieste, Italy

[‡]Department of Physics, Università degli studi di Trieste, Piazzale Europa 1, I-34127 Trieste, Italy

[§]Department of Condensed Matter Physics, University of Geneva, Rue du Général- Dufour 24, 1204 Geneva, Switzerland

Supporting Information

ABSTRACT: The branching ratio of the excited-state population at the conical intersection between the S_1 and S_0 energy surfaces (Φ_{CI}) of a protonated Schiff base of all-trans retinal in protic and aprotic solvents was studied by multipulse ultrafast transient absorption spectroscopy. In particular, pump–dump–probe experiments allowed to isolate the S_1 reactive state and to measure the photoisomerization time constant with unprecedented precision. Starting from these results, we demonstrate that the polarity of the solvent is the key factor influencing the Φ_{CI} and the photoisomerization yield.



INTRODUCTION

The conical intersections (CIs) are often encountered in the photoexcited reactions of polyatomic molecules, and they act as an efficient funnel enabling ultrafast internal conversion between different electronic states.^{1–3} However, understanding the passage of a polyatomic system through a CI, and especially the influence of the environment on this passage, remains a challenging problem.

In particular, the processes happening at CIs are of paramount importance for retinal proteins, since at this topological site, the excited-state population can decay into the reactant ground state or proceed along the isomerization path ending up in the product ground state.^{4,5} For example, rhodopsin (Rh) and bacteriorhodopsin (bR) convert the light into atomic scale mechanical motions through a photoisomerization process with a quantum yield (Φ_{ISO}) larger than 60%.^{6–9} In other words, the branching ratio of the excited-state population at the CI (Φ_{CI}), or cis/trans branching ratio, is directly responsible for the successfulness of the photoisomerization reaction. Therefore, the protonated Schiff base of retinal (PSBR), i.e., chromophore of retinal proteins, dissolved in various solvents is an excellent model system to investigate environmental effects on the processes inside and near the CI.

Here by using multipulse ultrafast transient absorption spectroscopy, we clearly show that the key factor in determining the Φ_{CI} of PSBR in liquid phase is the polarity of the solvent.

A three-step model (Figure 1a) is currently accepted to describe the excited-state dynamics in bR, as measured in time-resolved studies.^{4–6,10–12} In this model, the initial relaxation, after the photoexcitation, involves a double-bond expansion and a single-bond compression^{3,13} (<50 fs). The nuclear wave

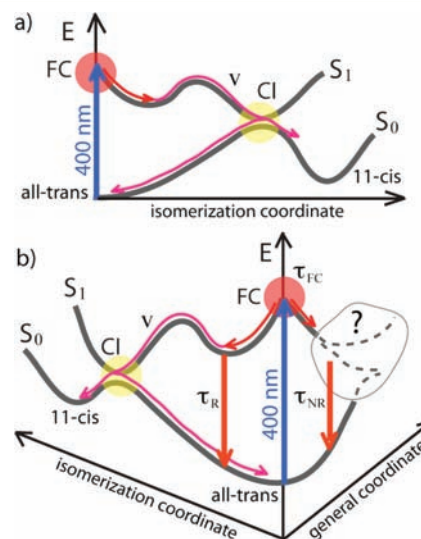


Figure 1. Three step models of the all-trans PSBR isomerization: (a) in bR and (b) in the solvent environment.

packet, prepared in the Franck–Condon (FC) region (Figure 1a, red area), continues to relax along the isomerization coordinate encountering a small activation barrier on the S_1 potential energy surface (PES). The barrier is at the origin of an excited-state intermediate, known in literature as the fluorescent state I.^{4,5,14,15} The molecules that surmount this barrier follow a barrierless isomerization path arriving to a peaked CI between the S_1 and the S_0 PES,^{3,16,17} as evidenced by

Received: June 21, 2011

Published: December 6, 2011

the yellow area on Figure 1a. The same model is valid also for Rh although, in this case, the barrier is very small.¹⁸

The photophysics of PSBR complicates in going from a protein to a solvent environment, where another branching close to the FC point appears.^{19,20} In this case the population splits between reactive and nonreactive channels (Figure 1b, red area).^{19,20} The reactive population, after the initial relaxation, follows the three-step-model as in the protein but with a slower dynamics.^{19–22} Therefore, due to the presence of nonreactive channel, assessing the value of Φ_{CI} is possible only if the reactive population is isolated while tracking the reaction routes at the CI topological site (Figure 1b, yellow area).

Concerning the nonreactive channel's nature and behavior, at the present, are not clear, and different models can be considered.²³ However, very preliminary hybrid quantum mechanics/molecular mechanics (QM/MM) calculations, that include the PSBR chromophore and two counterions for the QM part and the solvent molecules for the MM part, seem to suggest that the nonreactive channel could be the rotation of the β -ionone ring governed by low-energy barrier.²⁴ This mechanism is compatible with the suggestion of Olivucci et al.²³ that a tiny barrier on the S_1 surface modulates the decay of the excited-state population. Of course, a more advanced and complete modeling along with more extensive experiments are needed to clarify this point.

The origin of the microscopic mechanisms that influence the Φ_{CI} has been the matter of intense research in the last 20 years.

In bR and Rh, since there are no other channels on the way from the FC region to the CI, such ratio is equal to photoisomerization yield ($\Phi_{\text{CI}} = \Phi_{\text{ISO}}$) and assumes a high value of >60%. In earlier studies, the correlation between Φ_{ISO} (and Φ_{CI}) and the isomerization velocity has been rationalized in terms of a Landau–Zener transition^{25,26} through an avoided S_1/S_2 crossing.^{27–30} This has been supported by the observations that the high Φ_{ISO} (and high Φ_{CI}) in bR and Rh is accompanied by very fast (200–400 fs) isomerization and that PSBR in a solvent exhibits a slow down of dynamics to more than 2 ps^{19–22} while a 3-fold drop of Φ_{ISO} takes place.^{31–34}

Nonetheless, a doubt that a high diffusion speed of the wave packet is not sufficient to achieve high Φ_{CI} has started to emerge from a recent experimental study³⁵ along with other few computational studies^{36–39} that we will shortly discuss.

Recent experiments on a biomimetic photoswitch that mimics the photophysics of the retinal showed that Φ_{ISO} , also in this case equal to Φ_{CI} , remained low (<35%) although photoisomerization time constants were as fast as 200 fs. This result and previous studies^{36–39} suggested that static and dynamic tuning of the CI induced by the environment must be considered in condensed phase photochemistry. The static effects change the PES topography in the vicinity of the CI, while the dynamic ones mostly affect the path the wavepacket takes in approaching the conical funnel.

Static effects of the solvent have been noticed in calculations of the chromophores of green fluorescent protein (GFP)^{36,37} and photoactive yellow protein (PYP)³⁷ and of a model PSBR.^{37,40–42} The common feature in all these systems was that CIs were formed by intersections of two quantum states of charge-transfer and covalent character, respectively, so that solvent orientational degrees of freedom lead to selective solvation only of the charge-transfer state. Hence, the solvent was able to change geometry, topology, and energetics of the CI or even completely remove it.^{40,42} An ab initio study by Ben-

Nun and co-workers^{43,44} has shown that a change of the PES topology can induce substantial effects on Φ_{CI} of the PSBR chromophore in solution.

Regarding the dynamical solvent effects, Voll and co-workers⁴⁴ have calculated that in fulgides, the branching ratio can be substantially modified by changes of the pathways through the CI and/or by changes of the time-dependent potentials and/or changes of the dissipation processes. Recent quantum dynamics computational study of a model PSBR by Hynes and co-workers³⁸ showed how dynamical friction effects, related to the solvation velocity of the solvent molecules, are important factors in determining the final value of the cis/trans product ratio (Φ_{CI}). The latter study and previous study of Warshel and collaborators⁴⁵ demonstrate how simulations of the quantum mechanical dynamics is a good approach to quantitatively predict Φ_{CI} and Φ_{ISO} . However, experimental measurements of Φ_{CI} were lacking for PSBR dissolved in various solvents. Such measurements would allow clarifying the nature of the microscopic mechanisms that influence the Φ_{CI} .

In this paper we present an experimental study on PSBR in solution identifying the environmental effects on this branching ratio (Φ_{CI}). The selection between reactive and nonreactive populations was achieved by using a pump–dump–probe (PDP) transient absorption spectroscopy. This technique allows measuring the photoisomerization time constant (τ_{R}). Making use of both τ_{R} and the excited-state (S_1) relaxation dynamics, obtained from independent pump–probe (PP) measurements, it is possible to evaluate the relative population in the reactive state. Finally, using the Φ_{ISO} , that was previously measured by the high-performance liquid chromatography (HPLC) technique,³³ Φ_{CI} can be determined. By following this procedure, Φ_{CI} was found to be increasing with the solvent polarity, whereas no correlations between Φ_{CI} and τ_{R} were observed. This result can be rationalized considering that S_1 and S_0 states have very different charge distributions^{3,13,17,46} (and are of charge-transfer or covalent character, respectively) so that solvent dielectric properties have a significant impact both on the CI geometry and on the surrounding topology.^{37,40–42}

■ EXPERIMENTAL SECTION

The *n*-butylamine Schiff bases of all-trans retinal were prepared according to previously described methods²² and protonated using a three to five-fold excess of trifluoroacetic acid. The solutions were prepared starting from pure dried solvents, methanol (MeOH), acetonitrile (ACN), dichloromethane (DCM), and cyclohexane (cHex) and used as received. The sample steady-state absorption between 300 and 600 nm was measured by mean of a commercial spectrophotometer (Pharmacia Biotech Ultraspec 3000). The optical density (OD) as measured at the absorption maximum (444 in MeOH, 450 nm in ACN) for a 1 mm thick sample was 0.75–0.9. A 1 kHz regenerative amplifier was used to generate 50–60 fs pulses at 795 nm with an energy of ~ 0.6 mJ. By focusing a portion of the fundamental beam to a 2 mm thick CaF₂ crystal, a supercontinuum (SC) white light was generated.⁴⁷ The SC beam was split into the probe and the reference beam by using a metallic-coated beamsplitter. The probe beam alone was imaged onto the sample to a spot of a ~ 70 μm diameter, and it was in spatial–temporal coincidence with the pump and dump pulse at 400 and 800 nm, respectively, both having spot size on the sample ≥ 140 μm . Before arriving on the sample, both the pump and the dump beams were chopped at 250 Hz. The probe and the reference beams were then dispersed, after the interaction with the sample, on two 512 pixel diode arrays with a homemade spectrometer based on transmission grating. The diode arrays were integrating signals from two consecutive pulses, while control software

first sorted acquired spectra into the pumped and the unpumped group, and then each group was averaged out. For each time step 2000 shots were used. All the beams had identical polarization. The PP and the pump–dump delays were varied independently by means of two motorized translation stages. The intensities of the pump ($\sim 135 \mu\text{W}$) and the dump ($\sim 200 \mu\text{W}$) beams were chosen to achieve the linearity of the PP signal (variation of the optical density ΔOD) and of the damping amplitude. The dump pulse alone did not induce detectable transient absorption signal. By using a peristaltic pump, the sample was circulated through a quartz capillary (Vitrocom, 0.5 mm path length, 0.25 mm quartz window). The flow speed was chosen to ensure sample refreshment for each laser pulse.

RESULTS

For every solvent, transient difference absorption spectra were first collected in the standard broadband PP configuration. Figure 2 presents a transient absorption at 400 fs for PSBR in

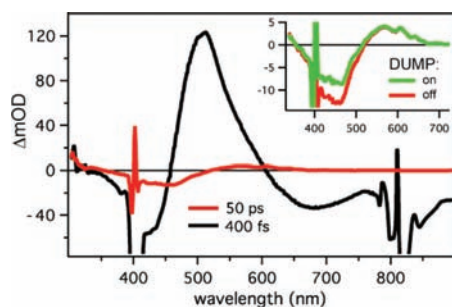


Figure 2. Transient absorption spectra obtained from the PP experiment. Inset: spectra at 50 ps with and without the dump pulse.

MeOH. All the spectral features expected for this system were detected. In the blue spectral region, the spectrum is dominated by a component having a negative ΔOD with a minimum at 430 nm. This feature is assigned to the S_0 ground-state bleach (GB) and to a partial overlap with the excited-state absorption (ESA) at 510 nm induced by the S_1 state.^{22,48,49} The red part of the latter absorption feature overlaps with the stimulated emission (SE) with a maximum at $\sim 700 \text{ nm}$.^{21,22,48,49} All these spectral features decay within $\sim 25 \text{ ps}$, leaving a relatively weak ($\sim 13 \text{ mOD}$) quasi-constant spectrum taken at 50 ps. This spectrum consists of a negative component under 530 nm and a positive component in the red. The negative component of the 50 ps spectrum is assigned to the “all-trans – cis” difference spectrum caused by the fact that the extinction coefficient halves in going from the all-trans to the cis isomer.^{31,32} Instead, a positive signal was observed for higher wavelengths (515 – 650 nm). According to Bismuth et al.,⁴⁸ this feature is assigned to metastable *s*-cis photoproducts.

To obtain the S_1 relaxation dynamics, we averaged the PP kinetic traces into $700 \pm 5 \text{ nm}$ range since in this region the response is due to SE only.^{19,49,50} The obtained traces (Figure 3) match well the excited-state decay traces resulting from fluorescence up-conversion measurements.^{19,50}

Once the retinal chromophore is brought from the ground to the excited state by pump photons at 400 nm, bond order change proceeds within $< 50 \text{ fs}$,⁵¹ leading to a sub-50 fs redshift of the SE¹⁹ by more than 6000 cm^{-1} . Consequently, the maximum of the SE is within few tens of femtoseconds centered around 700 nm and extends to $> 900 \text{ nm}$.¹⁹ Therefore, introduction of photons at 800 nm, having half the energy of the pump photons, dumps the S_1 population back to the S_0 state.

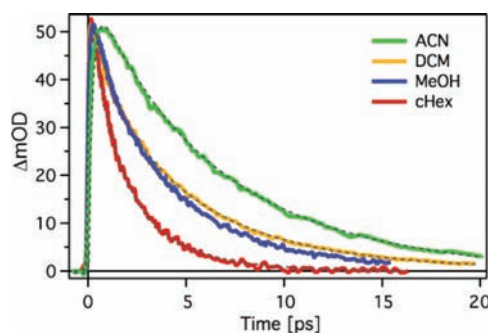


Figure 3. Kinetic traces at 700 nm from the PP scan and corresponding multiexponential fits (dashed lines). The curves are representing S_1 relaxation in various solvents.

By using the dump pulse concept, two multipulse spectroscopies have been performed. In the first spectroscopy, the pump–dump delay was kept fixed, and the probe was scanned in time. With this setup, the damping time constant and the percentage of the population dumped from the excited to the ground state were obtained from the PDP kinetic trace. Figure

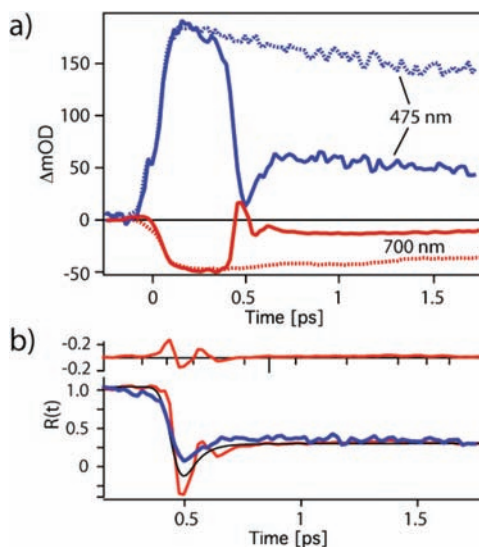


Figure 4. (a) Kinetic traces at 475 and 700 nm (ESA and SE, respectively) for PSBR in methanol with and without the dump pulse ($\Delta\text{OD}_{\text{dump}}$, solid line; $\Delta\text{OD}_{\text{no dump}}$, dashed line). (b) Traces $R(t) = [\Delta\text{OD}_{\text{dump}}/\Delta\text{OD}_{\text{no dump}}]$ for 475 and 700 nm (blue and red, respectively) and multiexponential fit curve of the latter (black). Upper graph reports residual of the multiexponential fitting of the $R(t)$ at 700 nm.

4a shows the PDP kinetic traces at 475 and 700 nm resulting from measurements where the dump delay was set at 500 fs. At these probing wavelengths, the time traces represent the dynamics of the ESA and SE spectral features, respectively.^{48,49} For reference, a trace taken without the dump is shown as well (Figure 4a, dashed lines). The ratios between the traces with and without the dump pulse $R(t) = [\Delta\text{OD}_{\text{dump}}/\Delta\text{OD}_{\text{no dump}}]$ are reported in Figure 4b. For delays $> 800 \text{ fs}$, the SE and ESA signals are depleted by the same amount ($\sim 66\%$). After the arrival of the dump pulse, the depletion of both features overshoots while approaching the asymptotic value of $\sim 66\%$ within $\sim 250 \text{ fs}$. A similar overshoot in the excited-state bleaching was observed in large organic molecules^{14,52} and halorhodopsin.⁵³ The overshoot of the SE feature was also

dressed up with oscillatory modulations that were extracted by subtracting the kinetic fits from the $R(t)$ trace (the fitting procedure is explained in detail in Supporting Information). A Fourier transform of the fit residual showed that one low-frequency mode at 210 cm^{-1} (fwhm 100 cm^{-1}) predominantly contributed to the modulations.

The PDP action traces were measured in the second spectroscopy setup. The effect of the pump–dump delay on a transient absorption, at a fixed PP delay, was detected, and the lifetime of the reactive S_1 state (τ_R), i.e., isomerization time constant of the all-trans \rightarrow 11-cis isomerization, was measured. The probe was fixed at a delay time of 50 ps with respect to the pump. For such delay, the S_1 internal conversion and photoproduct relaxation were over,^{22,48} and only the “all-trans – cis” difference spectrum (Fig. 2, red line) was observed. The intensity of this feature, which is directly proportional to the concentration of the photoproduct, was reduced (Figure 2, inset) from 12 to 7 mOD when the dump pulse arrived within τ_R . This proves that the dump pulse was perturbing the photoreaction.

Obtaining an action trace with a significant signal-to-noise ratio was challenging since the “all-trans – cis” spectrum had intensity that reduced only by ~ 5 mOD after the interaction with the dump pulse. More than 10 independent dump delay scans, with average scan duration of 25 minutes, were needed to obtain a significant signal to noise ratio. Eventually, from the fit of the PDP action trace (Figure 5) resulted by averaging traces

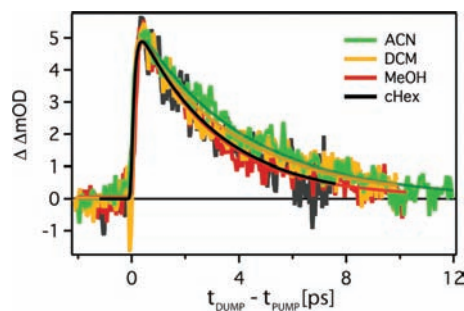


Figure 5. PDP action trace at 450 nm (averaged ± 15 nm) for the probe pulse fixed at 50 ps.

within 450 ± 15 nm (Figure 2, inset), τ_R was measured. In contrast with the overall S_1 decay, which is bi- or even triexponential, the PDP action trace was monoexponential for all solvents, showing that τ_R ranges from 2.8 ps for MeOH to 3.9 ps for ACN. In addition, it was necessary to include a 100–120 fs rise in the fit. This time scale is comparable to the 110–190 fs rise found in time resolved fluorescence experiments that was assigned to the “fill-up” time constant (τ_{FC} on Figure 1b) of the local minima on the S_1 hypersurface.¹⁹

Using this approach τ_R for different solvents was measured with an unprecedented precision (Table 1). The lifetime of the

nonreactive S_1 states (τ_{NR1} , τ_{NR2}) was then determined by fitting the S_1 decay with a bi- or triexponential function, while τ_R was kept fixed. Another degree of freedom was removed making the fit unequivocal and giving the fitting parameters with a significantly lower uncertainty respect to previous up-conversion studies.^{19–21} The lifetimes and the corresponding relative amplitudes of the reactive and the nonreactive channels (A_R , A_{NR1} , A_{NR2}) obtained from the fit are reported in Table 1. These amplitude data are particularly important since they represent the percentage of the reactive and nonreactive channel after the relaxation from the FC point.

In all solvents but ACN, a fast nonreactive state with $\tau_{NR1} = 0.6/1$ ps, and a relative amplitude A_{NR1} ranging from 18% (MeOH) to 59% (cHex) was observed. Instead, a slow nonreactive state with $\tau_{NR2} = 5.2/6.7$ and $A_{NR2} = 35/70\%$ was detected in all solvents but cHex. A_R was also observed, increasing by $\sim 25\%$ in going from polar (ACN, MeOH) to nonpolar solvents (cHex, DCM). All the molecules reaching the reactive state must pass through the CI where a further population branching occurs. A significant percentage (Φ_{CI}) will isomerize finishing in the cis-isomer, whereas the rest will return back to the initial all-trans configuration.

In principle, another pathway starting in the reactive minimum and ending in the reactant ground state, avoiding the CI responsible for isomerization, could be possible. Even if this hypothetical path was present, a monoexponential decay of the reactive population would be observed, since the total rate constant for parallel kinetics is equal to the sum of the rates of each channel. However, in the present experiment, as well in other studies reported in the literature,^{3,16,17} there is no evidence for such a parallel channel. Therefore, here the model that interprets the experimental data with the minimum number of parameters has been considered and used.

Knowing Φ_{ISO} from previous works^{31–33} and A_R the branching ratio at CI can be calculated from: $\Phi_{CI} = \Phi_{ISO}/A_R$. A clear increase of Φ_{CI} was detected as the solvent polarity (ϵ_r) was increased (Table 1). In particular, Φ_{CI} was 34% in the nonpolar cHex, increasing up to 39% in slightly polar DCM and 47% in MeOH, while reaching 90% in ACN.

DISCUSSION AND CONCLUSIONS

Main motivation for this PDP experiment was urged by the need of disclosing the mechanisms responsible for Φ_{ISO} enhancement observed in ACN. This problem could be addressed by determining with high-precision (uncertainty < 0.5 ps) τ_R of the all-trans PSBR photoreaction in solution, by considering the photoisomerization dynamics ($\sim 1/\tau_R$), and the amount of molecules ending in the reactive channel after leaving the FC zone.

In experiments using a conventional PP setup the main scope was obtaining the S_1 lifetimes for different solvents (Figure 3). The transient absorption data in MeOH reported in Figure 2 agree with the data measured in previous broadband PP

Table 1. Lifetimes and Relative Amplitudes of Nonreactive/Reactive Channels and Population Branching Ratio Φ_{CI} in the CI of All-Trans PSBR in Different Solvents

solvent	ϵ_r	Φ_{ISO}	τ_R /ps	A_R	τ_{NR1} /ps	A_{NR1}	τ_{NR2} /ps	A_{NR2}	Φ_{CI}
ACN	35.94	0.27 ± 0.04	3.9 ± 0.1	0.30 ± 0.04	–	–	7.8 ± 0.2	0.70 ± 0.03	0.90 ± 0.10
MeOH	32.66	0.17 ± 0.03	2.8 ± 0.1	0.36 ± 0.02	0.6 ± 0.1	0.18 ± 0.01	5.2 ± 0.2	0.46 ± 0.02	0.47 ± 0.09
DCM	8.93	0.17 ± 0.02	3.7 ± 0.1	0.45 ± 0.10	1.0 ± 0.2	0.21 ± 0.03	6.7 ± 0.7	0.35 ± 0.09	0.39 ± 0.10
cHex	2.02	0.14 ± 0.02	3.0 ± 0.2	0.41 ± 0.01	1.0 ± 0.2	0.59 ± 0.01	–	–	0.34 ± 0.05

studies.^{22,48} To our knowledge, previous PP studies in ACN, cHex, and DCM are not reported in the literature. However, the excited-state decay curves obtained in the present experiment by probing the stimulated emission (Figure 3) are very similar to those reported from fluorescence up-conversion studies.^{19,20}

The dump pulse “short circuits” the photoreactions by moving a part of the excited-state population to the ground state. It should be made clear that the dump pulse could not selectively dump the population residing only in the reactive channel, since the latter had practically identical $S_1 \rightarrow S_0$ energy as the nonreactive channel.¹⁹ Nevertheless, the fact that a part of the nonreactive population was dumped to the initial (all-trans) ground state did not influence the dynamics of the PDP action trace but only its amplitude. This result can be explained by considering that this part of the population would end up in the initial all-trans state even in the absence of the dump pulse.

The relative magnitude of depletion of SE and ESA was comparable, suggesting that only the $S_1 \rightarrow S_0$ and the $S_1 \rightarrow S_n$ transitions were involved after the interaction with the dump pulse. The initial overshoot of the dumping efficiency observed in the SE (700 nm trace, Figure 4) was assigned to S_0 wavepackets and S_1 localized “holes” both impulsively generated by the dump pulse. This mechanism is similar to the one observed for halorhodopsin.⁵³ The overshoot observed in the ESA (475 nm trace, Figure 4) is a signature of the S_1 localized “holes” only. The modulations at 210 cm^{-1} provided more detailed information on the origin of these coherent nuclear motions. Since the modulations were observed only in the SE, they must originate from the S_0 wavepackets. Resonance Raman spectra in the low-frequency range have been reported only for the 11-cis isomer.⁵⁴ However, it is reasonable to expect that spectra of the all-trans isomer to be similar. Accordingly, the modulations observed in the present study would be assigned to C–C torsions.

The 400 nm excitation initially generates population in the FC region on the S_1 and makes the chromophore more flexible.⁵⁵ The population subsequently relaxes along various C=C torsional coordinates and splits into reactive local minima on the S_1 potential surface^{19,20} (called stationary point, SP³) and into nonreactive channels. The fact that the PDP action trace in all solvents presented a monoexponential decay suggests that only one S_1 intermediate local minima is reactive. Although τ_R for the MeOH solution is the shortest, Φ_{ISO} for ACN is 50% larger than for the other solvents used for the present experiment. Instead, τ_R for ACN and DCM was comparable, but Φ_{ISO} for DCM is as low as that of MeOH³³ (Table 1).

The absence of correlation between τ_R and Φ_{CI} proves that simple Landau–Zener model^{25,26} is not applicable here. Instead, this problem has been addressed in refs 42 and 57 by introducing the nonadiabatic CIs.

The three-step model,^{4,5} in which a small activation barrier is present on the S_1 surface along the isomerization coordinate,⁴⁹ successfully explains the data obtained in the present experiment. The existence of the barrier has been confirmed in several experiments.^{22,49} In these experiments it was concluded that the barrier height determines the reactive rate and not the slope of the S_1 surface in the vicinity of the CI. The present results show that the influence of solvent on τ_R and barrier height is modest for PSBR in solution, although solvent properties change significantly (Table 1). Therefore, the reaction velocity is not the key factor in determining Φ_{ISO} .

Φ_{ISO} is directly influenced by population branching at two specific points on the S_1 potential energy surface, i.e., at the FC region and at the CI. The percentage of molecule finishing in the reactive state after the first branching at the FC region increases by at least 25% in going from polar to nonpolar solvents. Nonetheless, this increase in the reactive population is not reflected in the Φ_{ISO} enhancement. For cHex, the less polar of the solvents used in this study, the yield was half the yield found in ACN. The yield in DCM, having polarity and polarizability close to cHex, was similar to the yield found in the much more polar MeOH. These results unambiguously prove that for achieving an efficient photoisomerization, it is not sufficient to massively populate the reactive state.

Another very important factor is the percentage of the reactive population ending up in the cis-isomer ground state after the passage through the CI (Φ_{CI}). Population dynamics at higher dimensional CI is highly influenced by various chromophore-solvent couplings of different origins.^{42,44,56} Here, since Φ_{CI} rises with the rising of ϵ_r (Table 1), the coupling with the orientational polarization field of the environment, i.e. polar and polarizable solvent, becomes of paramount importance. Since the PSBR photoisomerization and the passage through CI involves the transfer of positive charges,^{57,58} the chromophore couples strongly to dielectric properties of the solvent.

This electrostatic interaction on a model PSBR in solution has been treated in theoretical–computational study of Burghardt and Hynes.^{40,42} They found that when the solvent dipole moment was kept “frozen” in equilibrium to the charge distribution of the S_1 state in the FC point, the CI topology changes from a “peaked” shape (for the isolated chromophore) to a “sloped” shape. Recent ab initio calculations by Martinez and co-workers used such a topology modification to rationalize the bond selectivity of all-trans PSBR in solution.⁴³ Moreover, they suggested that the branching ratio in the “peaked” CI is favored for isomerization efficiency with respect to the “sloped” CI. The last example demonstrates how static environmental effects, i.e., the change in the CI topology, can directly influence Φ_{CI} .

We note that polar solvent, after the FC transition is gradually adapting to a new charge distribution in the excited state, introduces an additional “tuning” mode.^{40,42} This mode is described by solvent coordinate that increases dimensionality of the CI.^{40,42} For example, the CI that was a point in vacuum becomes a CI seam in solvent.

Besides introducing a static effect, the solvent can also induce a perturbation of the dynamical character mostly affecting the wavepacket path while approaching the CI seam.^{38,42} We suggest that the change in Φ_{CI} observed in going from MeOH to ACN depends on these dynamic phenomena. Certainly, the bulk dielectric response cannot play a significant role since static dielectric constant and polarizability of MeOH and ACN are very similar.

Recent quantum dynamical simulations of a PSBR model (without the barrier on S_1) in polar solvents including dynamical friction effects have shown that the pathway from the FC zone to the CI seam is not the same in water and ACN.^{38,41,42} These two polar solvents have a “fast” and a “slow” solvation process, respectively. Different approaches to the CI seam resulted in a change of nonadiabatic transition location on the PES.³⁸ After this finding, it was concluded that solvation dynamics and friction intensity play a significant role in determining the cis/trans product ratio (i.e., Φ_{CI}).

The solvation in ACN, among all organic solvents studied by Horng and co-workers,⁵⁹ is dominated by the inertial component ($\approx 70\%$ amplitude). This component, originating from the interaction between the PSBR chromophore and solvent molecules in the immediate proximity,⁶⁰ is very fast (90 fs).⁵⁹ In MeOH the inertial contribution is even faster (30 fs), but it amounts up to 10% of the total solvation process.⁵⁹ Although it remains unclear which model could explain the increase of Φ_{CI} in ACN, these results suggest that such an increase is not connected to the collective (diffusive) relaxation of the solvent but rather to the interaction of the PSBR chromophore with the near-neighbor solvent molecules.

Here we report on ultrafast multipulse optical experiments on the protonated Schiff base of all-trans retinal aimed to reveal the mechanisms influencing photoisomerization yield (Φ_{ISO}). The experimental results have been interpreted in the frame of the three-step model where the excited-state population, after photoexcitation, relaxes along different torsional coordinates reaching several stationary points on the S_1 surface. To isolate the reactive state, PDP transient absorption measurements were performed. τ_R and its dependence on the solvent polarity were measured, and τ_R was slower in DCM and ACN (~ 3.8 ps) and faster for MeOH and cHex (~ 2.9 ps).

On the basis of these results, we prove that the branching ratio in the CI between the S_1 and S_0 surfaces (Φ_{CI}) is the key factor in determining the Φ_{ISO} of PSBR molecules in solution, while Φ_{CI} gets more favorable for isomerization as the solvent polarity increases. In particular, in ACN Φ_{CI} can be as high as 90%.

■ ASSOCIATED CONTENT

■ Supporting Information

Details of fit procedure of the $R(t)$ trace (Figure 4b) and the corresponding graph. Graphs of the fit residual and its Fourier transform spectrum. This material is available free of charge via the Internet at <http://pubs.acs.org>.

■ AUTHOR INFORMATION

Corresponding Author

goran.zgrablic@elettra.trieste.it

■ ACKNOWLEDGMENTS

This work was supported in part by the Italian Ministry of University and Research under grant nos. FIRB-RBAP045JF2 and FIRB-RBAP06AWK3 and by the European Community—Research Infrastructure Action under the FP6 “Structuring the European Research Area” Programme through the Integrated Infrastructure Initiative “Integrating Activity on Synchrotron and Free Electron Laser Science” contract no. RII3-CT-2004-506008. The authors would like to thank Prof. Stefan Haacke for his suggestions and advice in realization of this experiment and Dr. Nada Došlić for valuable comments and discussions on the manuscript.

■ REFERENCES

- (1) Klessinger, M.; Michl, J. *Excited States and Photochemistry of Organic Molecules*; VCH Publishers, Inc.: New York, 1995.
- (2) Yarkony, D. R. *Rev. Mod. Phys.* **1996**, *134*, 955–961.
- (3) González-Luque, R.; Garavelli, M.; Bernardi, F.; Merchán, M.; Robb, M. A.; Olivucci, M. *Proc. Natl. Acad. Sci. U.S.A.* **2000**, *97*, 9379–9384.
- (4) Hasson, K. C.; Gai, F.; Anfinrud, P. A. *Proc. Natl. Acad. Sci. U.S.A.* **1996**, *93*, 15124–15129.

- (5) Gai, F.; Hasson, K. C.; McDonald, J. C.; Anfinrud, P. A. *Science* **1998**, *279*, 1886–1891.
- (6) Dobler, J.; Zinth, W.; Kaiser, W.; Oesterhelt, D. *Chem. Phys. Lett.* **1988**, *144*, 215–220.
- (7) Schoenlein, R. W.; Peteanu, L. A.; Mathies, R. A.; Shank, C. V. *Science* **1991**, *254*, 412–415.
- (8) Kandori, H.; Furutani, Y.; Nishimura, S.; Shichida, Y.; Chosrowjan, H.; Shibata, Y.; Mataga, N. *Chem. Phys. Lett.* **2001**, *334*, 271–276.
- (9) Tittor, J.; Oesterhelt, D. *FEBS Letters* **1990**, *263*, 269–273.
- (10) Mathies, R. A.; Brito Cruz, C. H.; Pollard, W. T.; Shank, C. V. *Science* **1988**, *240*, 777–779.
- (11) Haran, G.; Wynne, K.; Xie, A.; He, Q.; Chance, M.; Hochstrasser, R. M. *Chem. Phys. Lett.* **1996**, *261*, 389–395.
- (12) Du, M.; Fleming, G. R. *Biophys. Chem.* **1993**, *48*, 101–111.
- (13) Altoè, P.; Cembran, A.; Olivucci, M.; Garavelli, M. *Proc. Natl. Acad. Sci. U.S.A.* **2010**, *107*, 20172–20177.
- (14) Ruhman, S.; Hou, B. X.; Friedman, N.; Ottolenghi, M.; Sheves, M. *J. Am. Chem. Soc.* **2002**, *124*, 8854–8858.
- (15) Schmidt, B.; Sobotta, C.; Heinz, B.; Laimgruber, S.; Braun, M.; Gilch, P. *Biochim. Biophys. Acta, Bioenerg.* **2005**, *1706*, 165–173.
- (16) Garavelli, M.; Bernardi, F.; Celani, P.; Robb, M. A.; Olivucci, M. *J. Photochem. and Photobiol., A* **1998**, *114*, 109–116.
- (17) Garavelli, M.; Celani, P.; Bernardi, F.; Robb, M. A.; Olivucci, M. *J. Am. Chem. Soc.* **1997**, *119*, 6891–6901.
- (18) Frutos, L. M.; Andruniow, T.; Santoro, F.; Ferré, N.; Olivucci, M. *Proc. Natl. Acad. Sci. U.S.A.* **2007**, *104*, 7764–7769.
- (19) Zgrablić, G.; Haacke, S.; Chergui, M. *J. Phys. Chem. B* **2009**, *113*, 4384–4393.
- (20) Zgrablić, G.; Voitchovsky, K.; Kindermann, M.; Haacke, S.; Chergui, M. *Biophys. J.* **2005**, *88*, 2779–2788.
- (21) Kandori, H.; Sasabe, H. *Chem. Phys. Lett.* **1993**, *216*, 126–132.
- (22) Hamm, P.; Zurek, M.; Röschinger, T.; Patzelt, H.; Oesterhelt, D.; Zinth, W. *Chem. Phys. Lett.* **1996**, *263*, 613–621.
- (23) Olivucci, M.; Lami, A.; Santoro, F. *Angew. Chem., Int. Ed* **2005**, *44*, 5118–5121.
- (24) Došlić, N.; Ruđer Bošković Institute, Zagreb, Republic of Croatia; private communication.
- (25) Landau, L. D.; Lifschitz, E. M. *Quantum Mechanics (Non-Relativistic Theory)*, 3rd ed.; Pergamon Press: Oxford, U.K., 1981.
- (26) Wittig, C. *J. Phys. Chem. B* **2005**, *109*, 8428–8430.
- (27) Peteanu, L. A.; Schoenlein, R. W.; Wang, Q.; Mathies, R. A.; Shank, C. V. *Proc. Natl. Acad. Sci. U.S.A.* **1993**, *90*, 11762–11766.
- (28) Schoenlein, R. W.; Peteanu, L. A.; Wang, Q.; Mathies, R. A.; Shank, C. V. *J. Phys. Chem.* **1993**, *97*, 12087–12092.
- (29) Wang, Q.; Schoenlein, R. W.; Peteanu, L. A.; Mathies, R. A.; Shank, C. V. *Science* **1994**, *266*, 422–4.
- (30) Wang, Q.; Kochendoerfer, G. G.; Schoenlein, R. W.; Verdegem, P. J. E.; Lugtenburg, J.; Mathies, R. A.; Shank, C. V. *J. Phys. Chem.* **1996**, *100*, 17388–17394.
- (31) Becker, R. S.; Freedman, K. J. *Am. Chem. Soc.* **1985**, *107*, 1477–1485.
- (32) Freedman, K. A.; Becker, R. S. *J. Am. Chem. Soc.* **1986**, *108*, 1245–1251.
- (33) Koyama, Y.; Kubo, K.; Komori, M.; Yasuda, H.; Mukai, Y. *Photochem. Photobiol.* **1991**, *54*, 433–443.
- (34) Zgrablić, G.; Ricci, M.; Novello, A. M.; Parmigiani, F. *Photochem. Photobiol.* **2010**, *86*, 507–512.
- (35) Briand, J.; Bräm, O.; Rahault, J.; Leonard, J.; Cannizzo, A.; Chergui, M.; Zanirato, V.; Olivucci, M.; Helbing, J.; Haacke, S. *Phys. Chem. Chem. Phys.* **2010**, *12*, 3178–3187.
- (36) Toniolo, A.; Olsen, S.; Manohar, L.; Martinez, T. J. *Faraday Discuss.* **2004**, *127*, 149–163.
- (37) Toniolo, A.; Granucci, G.; Martinez, T. J. *J. Phys. Chem. A* **2003**, *107*, 3822–3830.
- (38) Malhado, J. P.; Spezia, R.; Hynes, J. T. *J. Phys. Chem. A* **2011**, *115*, 3720–3735.
- (39) Kelly, A.; Kapral, R. I. *J. Chem. Phys.* **2010**, *133*, 084502.

- (40) Burghardt, I.; Cederbaum, L. S.; Hynes, J. T. *Faraday Discuss.* **2004**, *127*, 395–411.
- (41) Burghardt, I.; Cederbaum, L. S.; Hynes, J. T. *Comput. Phys. Commun.* **2005**, *169*, 95–98.
- (42) Burghardt, I.; Hynes, J. T. *J. Phys. Chem. A* **2006**, *110*, 11411–11423.
- (43) Ben-Nun, M.; Molnar, F.; Schulten, K.; Martinez, T. J. *Proc. Natl. Acad. Sci. U.S.A.* **2002**, *99*, 1769–1773.
- (44) Voll, J.; Kerscher, T.; Geppert, D.; de Vivie-Riedle, R. *J. Photochem. and Photobiol., A* **2007**, *190*, 352–358.
- (45) Warshel, A.; Chu, Z. T. *J. Phys. Chem. B* **2001**, *105*, 9857–9871.
- (46) Molnar, F.; Ben-Nun, M.; Martinez, T. J.; Schulten, K. *J. Mol. Struct.-Theochem* **2000**, *506*, 169–178.
- (47) Kovalenko, S. A.; Dobryakov, A. L.; Ruthmann, J.; Ernsting, N. P. *Phys. Rev. A* **1999**, *59*, 2369–2384.
- (48) Bismuth, O.; Friedman, N.; Sheves, M.; Ruhman, S. *Chem. Phys.* **2007**, *341*, 267–275.
- (49) Logunov, S. L.; Song, L.; El-Sayed, M. A. *J. Phys. Chem.* **1996**, *100*, 18586–18591.
- (50) Zgrablić, G.; *Solvent effects on the ultrafast dynamics of the retinal chromophore of Bacteriorhodopsin*, Ecole Polytechnique Fédérale de Lausanne: Lausanne, Switzerland, 2006.
- (51) Ye, T.; Gershgoren, E.; Friedman, N.; Ottolenghi, M.; Sheves, M.; Ruhman, S. *Chem. Phys. Lett.* **1999**, *314*, 429–434.
- (52) Cerullo, G.; Lüer, L.; Manzoni, C.; De Silvestri, S.; Shoshana, O.; Ruhman, S. *J. Phys. Chem. A* **2003**, *107*, 8339–8344.
- (53) Bismuth, O.; Komm, P.; Friedman, N.; Eliash, T.; Sheves, M.; Ruhman, S. *J. Phys. Chem. B* **2010**, *114*, 3046–3051.
- (54) Lin, S. W.; Groesbeek, M.; van der Hoef, I.; Verdegem, P.; Lugtenburg, J.; Mathies, R. A. *J. Phys. Chem. B* **1998**, *102*, 2787–2806.
- (55) Valsson, O.; Filippi, C. *J. Chem. Theory Comput.* **2010**, *6*, 1275–1292.
- (56) Kelly, A.; Kapral, R. *J. Chem. Phys.* **2010**, *133* (2), 084502.
- (57) Bonačić-Koutecký, V.; Koutecký, J.; Michl, J. *Angew. Chem., Int. Ed* **1987**, *26*, 170–189.
- (58) Bonačić-Koutecký, V.; Schoffel, K.; Michl, J. *Theor. Chim. Acta* **1987**, *72*, 459–474.
- (59) Horng, M. L.; Gardecki, J. A.; Papazyan, A.; Maroncelli, M. *J. Phys. Chem.* **1995**, *99*, 17311–17337.
- (60) Ladanyi, B. M.; Liang, Y. Q. *J. Chem. Phys.* **1995**, *103*, 6325–6332.